Energy Conversion and Management 277 (2023) 116650

Contents lists available at ScienceDirect

Energy Conversion and Management

journal homepage: www.elsevier.com/locate/enconman

Micro solid oxide fuel cell thermal dynamics: Incorporation of experimental measurements and model-based estimations for a multidimensional thermal analysis

Konstantinos Zoupalis [a], Amirpiran Amiri [a,*], Kate Sugden [a], Michaela Kendall [b], Kevin Kendall [b]

[a] Energy and Bioproducts Research Institute (EBRI), College of Engineering and Applied Science, Aston University, UK
[b] Adelan Ltd, Weekin Works, Harborne, UK

ARTICLE INFO

Keywords:
SOFC
Thermal dynamics
Positive-Electrolyte-Negative

ABSTRACT

Transient behaviour of solid oxide fuel cells during various stages of operation, such as warmup, startup, load fluctuations, and shutdown, must be understood and predicted in order to design an efficient controller and prevent degradation/failure of the cell. The difficulty of measuring and monitoring solid oxide fuel cell thermal features necessitates an evaluation of the solid oxide fuel cell thermal dynamics using a hybrid tool that integrates both experimental and numerical methods. In this study, a hybrid measurement tool consisting of a quasi-two-dimensional microscale model and a test rig was used to investigate the solid oxide fuel cell thermal dynamics. Through the hybrid experiment-model approach, steady-state temperature differences across Positive-Electrolyte-Negative and along fuel flow direction were captured. Additionally, the speed of temperature difference change was estimated in two dimensions, which is crucial when estimating transient thermal stresses. Several thermal measures were used to evaluate the thermal dynamics of solid oxide fuel cells. The impact of the operating voltage regime on solid oxide fuel cell thermal dynamics was studied using the varying operating voltage (Voltage Interrupted Measurement) characterisation approach. The outcomes revealed that optimising the performance of solid oxide fuel cells requires a trade-off between thermal management and fuel utilisation due to the exponential effect of fuel utilisation on steady-state temperature differences. The effects of fuel humidity and oxygen content of the oxidant flow on solid oxide fuel cell thermal dynamics were also examined. The results shed light on the new aspects of fuel cell thermal dynamics that are key in designing future smart controllers.

1. Introduction

The Solid Oxide Fuel Cell (SOFC) is a highly efficient device that directly converts fuels' chemical energy to electricity with a lower environmental impact than traditional energy solutions such as combustion engines [1]. Traditional energy generation paths use combustion to produce heat which is converted to kinetic energy and electrical power with a substantial loss for each step. In contrast, the SOFC converts fuel chemical energy directly into electrical energy through electrochemical reactions, while its efficiency is not limited to the Carnot efficiency. Therefore, its electrical efficiency can reach 60 % or higher. Utilising the waste heat can even promote overall (electrical and thermal) efficiency up to 82 % [2] and beyond. The noise-free operation makes the SOFC system ideal for residential applications [3]. Hydrogen fuelled SOFC is pollution-free as the electrochemical reaction product is water. The SOFC is fuel-flexible and capable of utilising renewable fuels such as natural gas, biogas, syngas [4], methanol [5], ammonia [6] and methane [7] to reduce carbon release.

To realise SOFC widespread deployment, the lifespan - also known as longevity and lifetime - should be prolonged to assure its reliability and economy. This is currently a serious technical challenge. The SOFC longevity has been the focus of extensive research in the last decade. The lifetime expectation for marketable SOFC varies depending on its application. Japan's New Energy and Industrial Technology Development Organization is currently running a long-term longevity study of SOFCs and has a target of 10 % performance loss over 10 years, i.e., 0.11 %/1000 h [8]. Similarly, the US Department of Energy's Solid State Energy Conversion Alliance has a target of 0.2 %/1000 h loss over 4.5 years lifetime [9]. Fundamental understanding and quantitative monitoring of SOFC degradation drivers are essential to realise these ambitious targets.

Temperature gradients, hot spots, fuel/air impurities, and

* Corresponding author.
E-mail address: a.p.amiri@aston.ac.uk (A. Amiri).

https://doi.org/10.1016/j.enconman.2022.116650
Received 11 July 2022; Received in revised form 27 December 2022; Accepted 30 December 2022
Available online 5 January 2023

Nomenclature

Notes

T_x (t)	transient local temperature along the cell length
T_y (t)	transient local temperature across the PEN
ΔT_x (t)	transient temperature difference along the cell length (T_{x1} (t) – T_{x2} (t))
ΔT_y (t)	transient temperature difference across the PEN (T_{y1} (t) – T_{y2} (t))
$\Delta T_{x,ss}$	steady-state temperature difference along the cell length (ΔT_x (t) at t > settling time)
$\Delta T_{y,ss}$	steady-state temperature difference across the PEN (ΔT_y (t) at t > settling time)

Abbreviations

AGR	Anode exhaust gas recycling
BoP	Balance of Plant
OCV	Open Circuit Voltage
OEA	Oxygen enriched air
PEN	Positive electrode - Electrolyte - Negative electrode
SOFC	Solid Oxide Fuel Cell
OP	Overpotential
VIM	Voltage Interrupted Measurement
POX	Partial oxidation reaction
k^s_{eff}	Species effective mass transfer coefficient (m/s)
D^s_{eff}	Species effective mass diffusivity coefficient K (m^2 s^{-1})
D^s_{298}	Species effective mass diffusivity coefficient at 298 K (m^2 s^{-1})
$\dot{N}$	Mass transfer rate from sub-systems boundaries to other sub-system
$\dot{Q}$	Heat transfer rate to/from the sub-system
C_{dL}	Double layer capacitance (A s/V m^{-2})
C_h	Channel height (m)
CO	Carbon monoxide
CO_2	Carbon dioxide
C_p	Specific heat capacity (Jmol^{-1} K^{-1})
d(ΔT)/dt	The speed of temperature difference change
E_{act}	Activation energy (kJ/mol)
E_{cell}	Cell voltage (V)
E^{OCV}	Open circuit voltage based on the Nernst equation (V)
F	Faraday's constant (96,485 Cmol^{-1})
F_{in}	Inlet molar flow rate (mol s $^{-1}$)
F_{out}	Outlet molar flow rate (mol/s)
H	Specific enthalpy (J/mol) & Humidity (%)
H_2	Hydrogen
H_2O	Water
I	Current (A)
i	Current density (A/m^{-2}(−|-))
i*	Pre-exponential kinetics factor (A/m^{-2}(−|-))
i_o	Exchange current density (A/m^{-2}(−|-))
n_e	Number of electrons
q	Energy source term (J/s)
R	Ideal gas constant (J/mol K^{-1})
r	Mass source term (mols s^{-1})
R^{ohmic}	Ohmic resistance term (Ω m^2)
S	Cell area (m^2)
T	Temperature (K)
t	Time (s)
T_x (t)	Transient local temperature along the cell length
T_y (t)	Transient local temperature across the PEN
U_f	Fuel utilisation
U_A	Air utilisation
V	Volume (m^3)
y	Species mole fraction
ΔH_R	Reaction enthalpy (J/mol)
$\Delta T_{s.s}$	Steady-state temperature differences
FH	Energy transfer at element inlet/outlet
yF	Species convective delivery

Greek Letters

α^C_A	Anodic charge transfer coefficient for cathode
α^A_A	Anodic charge transfer coefficient for anode
α^A_C	Cathodic charge transfer coefficient for anode
α^C_C	Cathodic charge transfer coefficient for cathode
$\boldsymbol{\rho_{mol}}$	Molar density (mol/m^{-3}(−|-))
α	Heat transfer coefficient (W/m^{-2}(−|-) K $^{-1}$)
γ	Reaction rate exponent
δ	Catalyst thickness (m)
ε	Porosity
η	Overprotection (V)
ν	Stoichiometric coefficient
ρC p^{PEN}	PEN thermal capacity (J/m^{-3}(−|-) K^{-1})
σ	Conductivity (Ω^{-1} m^{-1})

Sub/superscripts

A	Anode
α	Air
as	Air species
C	Cathode
cat	Catalyst layer
eff	Effective
eq	Equilibrium
f	Fuel
gas	Gas phase
in	Inlet
out	Outlet

mechanical stresses/failures are key contributors to the SOFC degradation, and hence its lifetime reduction. One of the major contributors to the SOFC degradation is thermal stress [10] caused by temperature gradients and thermal dynamics. The temperature gradient causes different magnitudes of expansion across a component with very low-temperature regions experiencing contraction. This causes the low-temperature region to suffer compression stress by the expanding high-temperature region. The high-temperature region is exposed to tensile stress by the contracting low-temperature region. Thermal stresses are also caused by the difference between the operating temperature and the zero-stress temperature. At zero-stress temperature, there are no residual stresses. However, if the temperature is less than the zero-stress temperature, residual stresses are still present due to variations in deformation for each component caused by differences in mechanical properties. It has been found that the contributions of these factors varied depending on the location in the fuel cell [11]. The temperature gradient and the difference between the operating temperature and zero-stress temperature dominate the low-temperature region. However, in higher temperature regions the temperature gradient becomes less significant [12]. The ceramics used in the construction of SOFCs are fragile, making them susceptible to creep, rupture and cracking when put under stress. Keeping the thermal and mechanical stresses placed on the SOFC components within tolerable limits is essential to maximising lifespan. Due to the connected nature of fuel cells in a stack, a single cell failure can cause stack malfunction. The SOFC can operate with the presence of minor cracks; however, there will be an effect on the performance of the cell. The local hot spots and temperature gradient can destroy the SOFC structure physically, hence thermal management is important to mitigate thermal stress [13].

The capabilities for the measurement of SOFC thermal performance

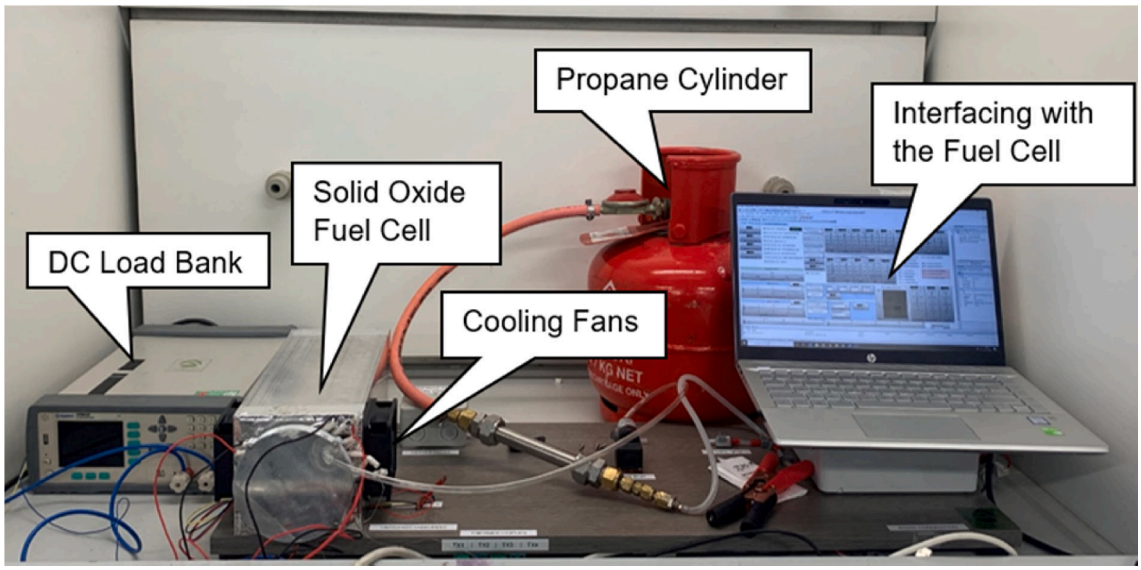

Fig. 1. Thermal test rig.

are currently limited to measuring technologies and techniques. At the *meso*-scale and macro-scale the temperature measurement, and hence the thermal gradients estimations, is technically feasible to a reasonable level. Razbani et al., [14] have experimentally measured the temperature profile over the cell surface for a SOFC short stack of six cells by using five thermocouples inserted inside the stack. In addition, Canavar et all., [15] measured the temperature distribution on the cell of a SOFC using woven meshes instead of using the machined process for the gas flow channel. Sugihara et al., used an infrared camera for measurement [16] at the micro-scale. The experimental measurements are extremely challenging and even impossible in most cases [17]. This is because of sensor specifications and sealing issues. Alternatively, an indirect measure has been used in some studies. For instance, in Fardadi et al., [18] the measurable temperature of the plate has been used as an approximate temperature of the Positive-Electrolyte-Negative (PEN). Montanini et al., [17], have applied infrared thermal imaging for temperature measurement at the cathode surface. The method has been applied to a specially designed SOFC, but without measuring temperature in dynamic mode.

Numerical tools are vital for thermal behaviour studies at all scales, particularly at the micro-scale. They can provide insight that is not possible through practical tests. Tang et al., proposed a computational pseudo-3D model for a multi-layer SOFC at a constant temperature that was validated against experimental data [19]. Amiri et al., developed a model to simulate a planar SOFC at both the stack and the system scales [20] with a focus on the SOFC thermal management. Most of the models used for SOFC thermal management are steady-state models [21]. Whilst they are extremely useful for capturing internal hotspots and non-uniformities in the steady-state operation of SOFC, the thermal dynamics are not taken into account. This is a critical shortage as thermal dynamics has been proven to be a dominant mechanism in SOFC control as is key to degradation monitoring and mitigation. The temperature dynamics play the main role in the SOFC speed in responding to various perturbations such as load variation, feed disturbance, etc. The current work aims to fill this gap by providing real-time data that can be used for time-dependent thermal stress analysis. As result, temperature-driven degradation analysis will be possible during transient processes such as startup and shutdown steps. For scale up [22] and integrated-systems optimisation [23] studies, the thermal dynamics aspects at the system level is the leading shortage, requiring further work to enhance the capabilities of the presented models.

This work contributes to important challenges relevant to SOFC thermal behaviour including:

(i) some aspects of SOFC thermal behaviour are not measurable;
(ii) the SOFC thermal behaviour is a complex issue that must be mapped alongside the operating condition regions;
(iii) and SOFC thermal features are not well considered in many efficiency-improving strategies proposed in the literature.

To address these challenges, this paper proposes a new approach to looking at SOFC thermal behaviour emphasising thermal dynamics. This innovative method consists of the following components:

(i) the measurable thermal behaviour was captured through an experiment supported by a first principle model for capturing unmeasurable variables. The impact of this approach will be beyond this paper. For instance, it is greatly applied to develop hybrid models, in which data from experiments, first principle models and data-driven models (e.g., machine learning models) will be utilised to offer solutions for complex technical problems;
(ii) the voltage regime map is introduced and applied to rigorously evaluate the thermal dynamics of SOFC throughout a wide operating voltage spectrum for voltage interrupted measurement (VIM) scenarios.
(iii) promising efficiency and health-improving techniques were explored from SOFC thermal behaviour viewpoint.

This work provides new knowledge relevant to the effect of the operating conditions on the SOFC thermal dynamics resulting in time-dependent data. Such data and insights can promote the future controllers' design. The SOFC thermal dynamics were simulated in two directions including the fuel flow and across the PEN. While the former was experimentally possible, the latter became achievable only by applying a detailed mathematical model. The proposed model was detailed enough to capture the PEN internal variables in dynamic mode. As such, the temperature was computed as a highly non-linear function of fuel cell parameters, operation variables, and involved transport/reaction mechanisms. The spatiotemporal temperature and thermal gradients were evaluated.

2. Methods

The thermal behaviour of the SOFC system was captured through experimental and modelling measurements.

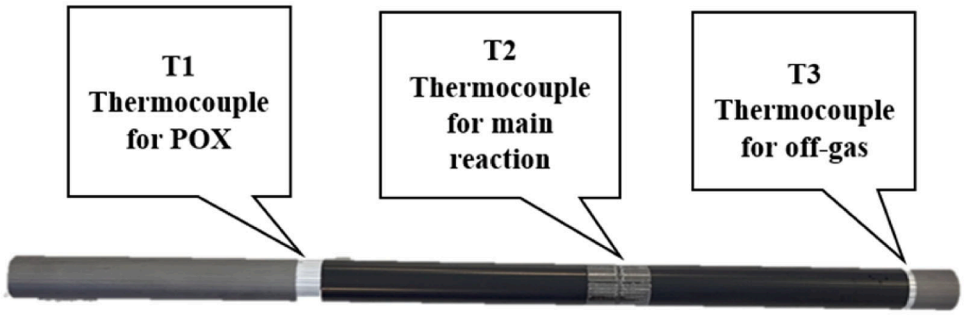

Fig. 2. SOFC tube thermocouple locations.

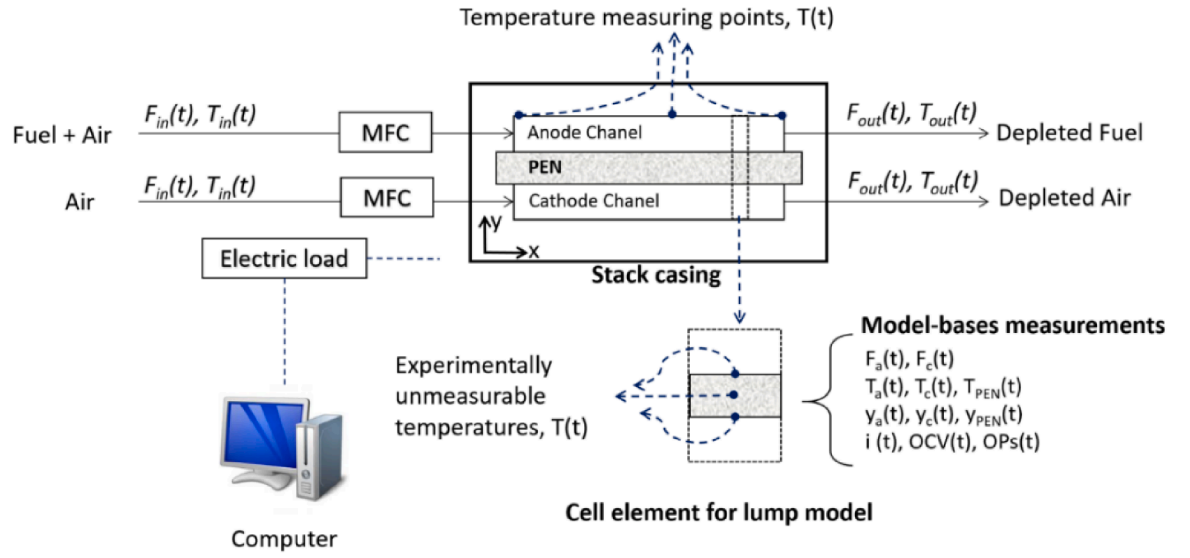

Fig. 3. Test rig schematic noted for physical model.

2.1. Test rig and model schematic

The test rig and a micro-tubular SOFC used in this work are shown in Figs. 1 and 2, respectively.

The model schematic is presented in Fig. 3.

2.2. Model development and validation

Following assumptions were used for model development:

- The model is semi-two dimensional (2D) and dynamic. It captures variables' changes at cell inlet/outlet and across the PEN.
- The fuel consists of hydrogen and steam. Air was used as an oxygen supply and coolant. Enriched air was used for further analysis purposes.
- The solid material properties and dimensions do not change with time and operating conditions.
- No internal fuel reformation was considered.

Three sub-systems were considered the main elements of the model. The corresponding control volumes are the anode (fuel) channel, cathode (air) channel, and PEN. The mass, energy and charge balances were computed for each sub-system.

The components balance in each sub-system were written according to the Equation (1);

$$\rho V\frac{dy}{dt} = (yF)_{in} - (yF)_{out} - \dot{N} \tag{1}$$

Where the mass transfer rate from sub-systems boundaries to another sub-system ($\dot{N}$) occurs mainly through diffusion mechanism, and yF stands for species convective delivery, due to the gas flow, at each element inlet/outlet. Application of the generic Equation (1) for all species involved leads to a set of ordinary differential equations.

The energy balance for each sub-system was computed by using a generic form as presented in Equation (2).

$$\rho VC_p\frac{dT}{dt} = (FH)_{in} - (FH)_{out} + \dot{Q} \tag{2}$$

where $\dot{Q}$ is the heat transfer rate to/from the sub-system and FH stands for energy transfer at element inlet/outlet due to gas flow.

The PEN energy balance was written as presented in Equation (3).

$$\rho VC_p\frac{dT^{PEN}}{dt} = \left(-\frac{\Delta H_R}{2F} - E_{Cell}\right)I + \left(S\alpha^a + \frac{C_p^{H_2} - C_p^{H_2O}}{2F}\right)(T^a - T^{PEN}) + \left(S\alpha^c + \frac{C_p^{O_2}}{2F}\right)(T^c - T^{PEN}) \tag{3}$$

Table 1
The extended governing and constitutive equations for individual sub-systems.

Component balances	
$\rho^{f}_{mol}V^{f}_{gas}\frac{dy^{fs}}{dt} = y^{fs}_{in}F^{f}_{in} - y^{fs}_{in}F^{f}_{out} - \rho^{f}_{mol}k^{fs}_{eff}S(y^{fs} - y^{fs}_{cat})$	Component balance in anode channel
$\rho^{a}_{mol}V^{a}_{gas}\frac{dy^{as}}{dt} = y^{as}_{in}F^{a}_{in} - y^{as}_{in}F^{a}_{out} - \rho^{a}_{mol}k^{as}_{eff}S(y^{as} - y^{as}_{cat})$	Component balance in cathode channel
$\rho^{f}_{mol}V^{f}_{cat}\frac{dy^{fs}_{cat}}{dt} = \rho^{f}_{mol}k^{fs}_{eff}S\left(y^{fs} - y^{fs}_{cat}\right) + r^{fs}$	Component balance for anode electrode
$\rho^{a}_{mol}V^{a}_{cat}\frac{dy^{as}_{cat}}{dt} = \rho^{a}_{mol}k^{as}_{eff}S\left(y^{as} - y^{as}_{cat}\right) + r^{as}$	Component balance cathode electrode
Energy balances	
$\rho^{f}_{mol}V^{f}_{gas}C^{f}_{p}\frac{dT^{f}}{dt} = (F^{f}_{in}H^{f}_{in} - F^{f}_{out}H^{f}_{out}) + q^{f}$	Energy balance: Anode channel
$\rho^{a}_{mol}V^{a}_{gas}C^{a}_{p}\frac{dT^{a}}{dt} = (F^{a}_{in}H^{a}_{in} - F^{a}_{out}H^{a}_{out}) + q^{a}$	Energy balance: Cathode channel
$\rho V^{PEN}C^{PEN}_{p}\frac{dT^{PEN}}{dt} = q^{PEN}$	Energy balance: PEN
Charge balance	
$C^{A}_{dL}\frac{d\eta_{A}}{dt} = (i_{cell} - i^{A})$	Charge balance anode/ electrolyte interface
$C^{C}_{dL}\frac{d\eta_{C}}{dt} = (-i_{cell} - i^{C})$	Charge balance cathode/ electrolyte interface
Constitutive equations	
$F^{a}_{Out} = F^{a}_{in} - \sum\rho^{f}_{mol}k^{as}_{eff}S(y^{as} - y^{as}_{cat})$	Air flow rate change
$F^{f}_{out} = F^{f}_{in} - \sum\rho^{f}_{mol}k^{fs}_{eff}S(y^{fs} - y^{fs}_{cat})$	Fuel flow rate change
$k^{s}_{eff} = D^{s}/C_{h}$	Species effective mass transfer coefficient
$D^{s} = D^{s}_{298}\epsilon^{1.5}\left(\frac{T}{298}\right)^{1.5}$	Species diffusivity
$i^{A} = i^{A}_{0}\left[exp(\frac{\alpha^{A}_{A}F(\eta^{A} - \eta^{A}_{eq})}{RT}) - exp(\frac{-\alpha^{A}_{C}F(\eta^{A} - \eta^{A}_{eq})}{RT})\right]$	Anode local current density
$i^{C} = i^{C}_{0}\left[exp(\frac{\alpha^{C}_{A}F(\eta^{A} - \eta^{A}_{eq})}{RT}) - exp(\frac{-\alpha^{C}_{C}F(\eta^{A} - \eta^{A}_{eq})}{RT})\right]$	Cathode local current density
$i^{A}_{0} = i^{*}_{A}(y^{H_2}_{cat})^{\gamma H_2}(y^{H_2O}_{cat})^{\gamma H_2O}exp(-\frac{E^{A}_{act}}{RT})$	Anode exchange current density
$i^{C}_{0} = i^{*}_{C}(y^{O_2}_{cat})^{\gamma O_2}exp(-\frac{E^{C}_{act}}{RT})$	Cathode exchange current density
$i^{cell} = (E^{OCV} - E_{cell} - \eta^{A}_{act} + \eta^{C}_{act})/R^{Ohmic}$	Electrolyte current
$\eta^{A}_{act} = \eta^{A} - \eta^{A}_{eq}$	Anode activation overpotential
$\eta^{C}_{act} = \eta^{C} - \eta^{C}_{eq}$	Cathode activation overpotential
$R^{Ohmic} = \delta_{e}/\sigma_{e}$	Electrolyte Ohmic resistance
$\sigma_{e} = 3.34 \times 10^{4}exp(-\frac{10300}{T})$	Electrolyte conductivity
$r^{H_2O} = S\frac{v^{H_2O}i^{A}}{n^{A}_{e}F}$	Water production rate
$r^{O_2} = S\frac{v^{O_2}i^{C}}{n^{C}_{e}F}$	Oxygen consumption rate
$r^{H_2} = S\frac{v^{H_2}i^{A}}{n^{A}_{e}F}$	Hydrogen consumption rate
$q^{f} = \alpha^{f}S(T^{PEN} - T^{f})$	Fuel channel heat transfer
$q^{a} = \alpha^{a}S(T^{PEN} - T^{a})$	Air channel heat transfer
$q^{PEN} = (-\frac{\Delta H_{R}}{2F} - E_{cell})I + \left(S\alpha^{f} + \frac{(C^{H_2}_{p} - C^{H_2O}_{p})}{2F}I\right)(T^{f} - T^{PEN}) + \left(S\alpha^{a} + \frac{C^{O_2}_{p}}{4F}I\right)(T^{a} - T^{PEN})$	PEN energy balance (net rate of energy accumulation)
$U_{F} = 1 - \frac{y^{H_2}_{out}F^{A}_{out}}{y^{H_2}_{in}F^{A}_{in}}$	Fuel utilisation
$U_{A} = 1 - \frac{y^{O_2}_{out}F^{C}_{out}}{y^{O_2}_{in}F^{C}_{in}}$	Air utilisation

The heat generated in the electrochemical reaction is transferred to the anode and cathode sides. During the transient phases, the net heat accumulation in PEN is not zero which results in a time-depended temperature.

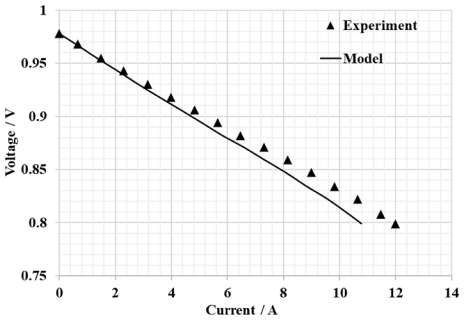

Fig. 4. Comparison of V-I data captured by applying the proposed model against the practical data from real-life tests.

The charge balance at anode/electrolyte and cathode/electrolyte interfaces can be presented as per Equations (4).

$$C^{A/C}_{dL}\frac{d\eta_{A/C}}{dt} = (i_{cell} - i^{A/C}) \quad (4)$$

The extended version of the balance equations and the constitutive equations for individual sub-systems are presented in Table 1.

The V-I profile was used to validate the model performance (Fig. 4). The figure illustrates that the mathematical model can capture the practical V-I data. The V-I profile is a strongly nonlinear function of temperature. It, therefore, can be concluded that the model's performance in estimating the temperature is reasonable.

3. Results and discussions

The temperature and temperature difference between two points can reach a steady-state value subject to enough time. The following terms are used in this paper to assess the thermal behaviour of the cell. The transient local temperature along the cell length, T_x (t); the transient local temperature across the PEN, T_y (t); the transient temperature difference along the cell length, ΔT_x (t); the transient temperature difference across the PEN, ΔT_y (t); the steady-state temperature difference along the cell length, $\Delta T_{x,ss}$; the steady-state temperature difference across the PEN, $\Delta T_{y,ss}$. The variation of temperature difference with time is given by $\Delta T/\Delta t$, which is a crucial term in the real-time evaluation of thermal stresses.

The dynamic temperature gradients formed across the SOFC dimensions are created by highly nonlinear interactions between several heat sources and sinks. The heat sources include the electrochemical reaction occurring at the three-phase boundary and the ohmic polarisation loss. As such, most of the heat is generated inside the PEN near the electrode/electrolyte interface. The internal fuel reforming, which takes place when SOFC is fed by fuels rather than pure hydrogen, can be either a heat source or sink. For instance, the partial oxidation (POX) of hydrocarbon fuels and gas-shift reaction (for carbon monoxide fuel) are extra heat sources in the PEN subsystem. In addition to heat losses to the environment and the coolant (air) to moderate the SOFC temperature at the allowed level, the endothermic internal fuel reformation process such as steam reforming of hydrocarbons, e.g., methane and propane, acts as the internal heat sinks. The temperature distribution, gradient and dynamics are ultimately dominated by the interaction of all processes.

In modelling work conducted by Ahmed & Foger [24] the internal distribution of steady-state temperature over a dimensionless axial distance was investigated. Amiri et al [20] have studied the thermal behaviour of SOFC estimating steady-state internal distributions in different layers of the cell structure including cathode, anode, electrolyte, and interconnects. The thermal dynamics, however, was not taken into account in the abovementioned studies. In this work, the data achieved from experimental tests and numerical model were used to fill

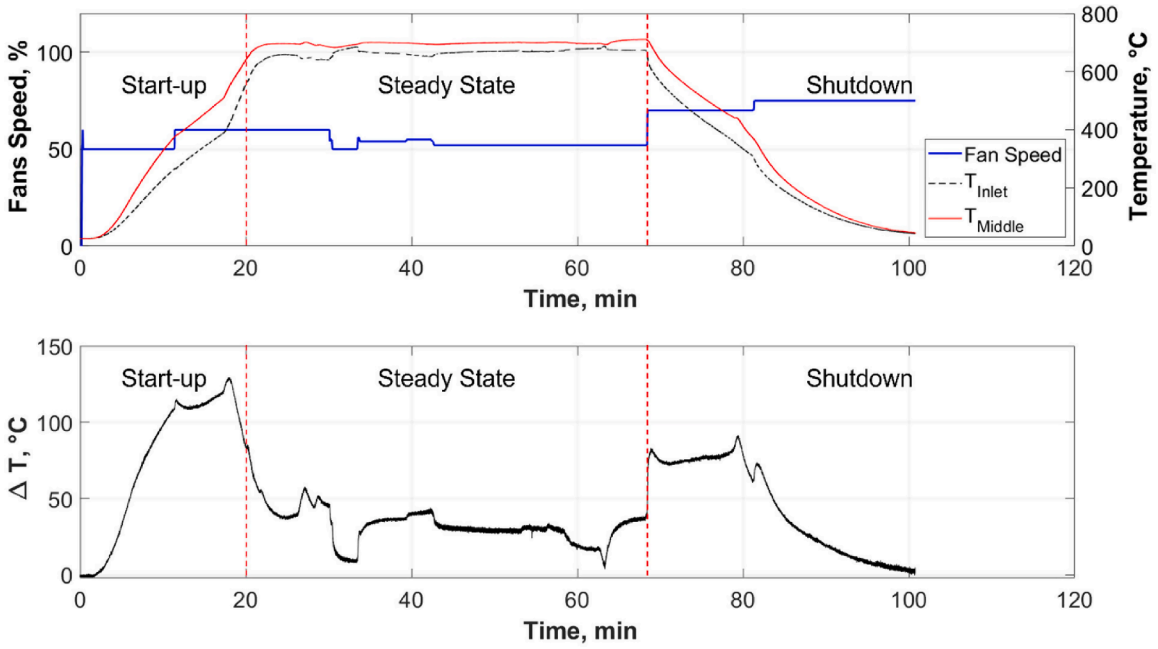

Fig. 5. The temperature dynamics and cooling fan function rate. (a) temperature dynamics along the cell tube, T_x, at two points captured by thermocouples #1 and #2; (b) transient local temperature difference along the cell length, $\Delta T_x(t)$, between thermocouples #1 and #2.

Table 2
Model parameters.

Parameter	Anode	Cathode
Catalyst thickness δ, m	2.5×10^{-4}	3×10^{-5}
Porosity ε	0.4	0.4
Charge transfer coefficient α_A	2	1.4
Charge transfer coefficient α_C	1	0.6
Activation energy E_{act}, kJ/mol	120	130
Pre-exponential kinetics factor i^*, A/m^{-2}(−|-)	2.9×10^8	7.0×10^8
Heat transfer coefficient α, W/m^{-2}(−|-) K^{-1}	25	25
Fluid physical properties	Calculated by Aspen Plus	
Channel height C_h, m	7.5×10^{-4}	
Cell area S, m^2	5×10^{-3}	
Electrolyte thickness δ_e, m	1×10^{-5}	
PEN thermal capacity ρc_p^{PEN}, J/m^{-3}(−|-) K^{-1}	106	
Species diffusivity at 298 K D^s_{298}, m^2 h^{-1}	0.22 (H_2), 0.079 (H_2O), 0.04 (O_2)	
Stoichiometric coefficient ν	–1 (H_2), 1 (H_2O), –0.5 (O_2)	
Reaction rate exponent γ	1.0 (H_2), 1.0 (H_2O), 0.25 (O_2)	
Operating conditions		
Cell voltage E_{cell}, V	0.80 (varying in VIM cases)	
Fuel flow rate F^f_{in}, ml min^{-1}	100	
Air flow rate F^a_{in}, ml min^{-1}	1000	
Fuel composition y, mole fraction		
Hydrogen (H_2)	0.97 (varying in VIM cases)	
Propane (C_3H_8)	0	
Water (H_2O)	0.03 (varying in VIM cases)	
Carbon Monoxide (CO)	0	
Carbon Dioxide (CO_2)	0	
Fuel inlet temperature, K	923	
Air inlet temperature, K	923	
Streams and SOFC pressure, atm	1	

this gap. The real-time mechanisms were simulated in this work to accurately capture the 2D thermal dynamics. The temperature dynamics in fuel flow direction was measured experimentally while the model-based estimation was conducted for data capturing across the PEN body. For the experimental part, the unsteady temperature was caused by startup and shutdown processes while for the model-based investigations the operating voltage change was used to induce the unsteady temperature in the system.

3.1. Thermal behaviour along the anode channel

Cell temperatures were experimentally measured at two different points of the tube during startup, normal (stabilised), and shutdown operations. The coolant air was used to control the temperature with its flow varying with the temperature change rates. The experimentally measured real-time temperature and temperature gradient dynamics along the cell tube (fuel flow or x-direction) are presented in Fig. 5. As shown in this figure, the fan speed fluctuation was required to ensure a gentle warm-up ramp, steady-state operation and even the cooling during the shutdown step, revealing that the coolant flow must be updated in a feedback control strategy. Over the test time, a substantial temperature difference between the two measuring points was observed for all three steps (Fig. 5a). In particular, the results reveal that while the cell experienced a temperature gradient (ΔT_x (t)) lower than 130 °C over most of the operation time, including startup and shutdown steps, the cell may suddenly experience a high gradient of thermal change. Therefore, fluctuations may occur in a short timeframe and they may impact the cell's performance and health in the mid- and long-term. This is because a high thermal disruption in a short time is a thermal shock that will promote cell degradation when the thermal cycle frequency is high, as in automotive applications.

3.2. Thermal behaviour across the electrodes and electrolyte

The state transition from one steady-state operation condition to another causes significant concerns for failure. The startup and shutdown steps are two severe state transitions. In assessing these transitional states both magnitude and speed of transition are crucial. The transient temperature and dynamics gradient in PEN were estimated using the model inputs presented in Table 2.

3.3. Voltage interruption simulation for base voltage impact

The time-dependent (ΔT_y) across the PEN was considered as a crucial

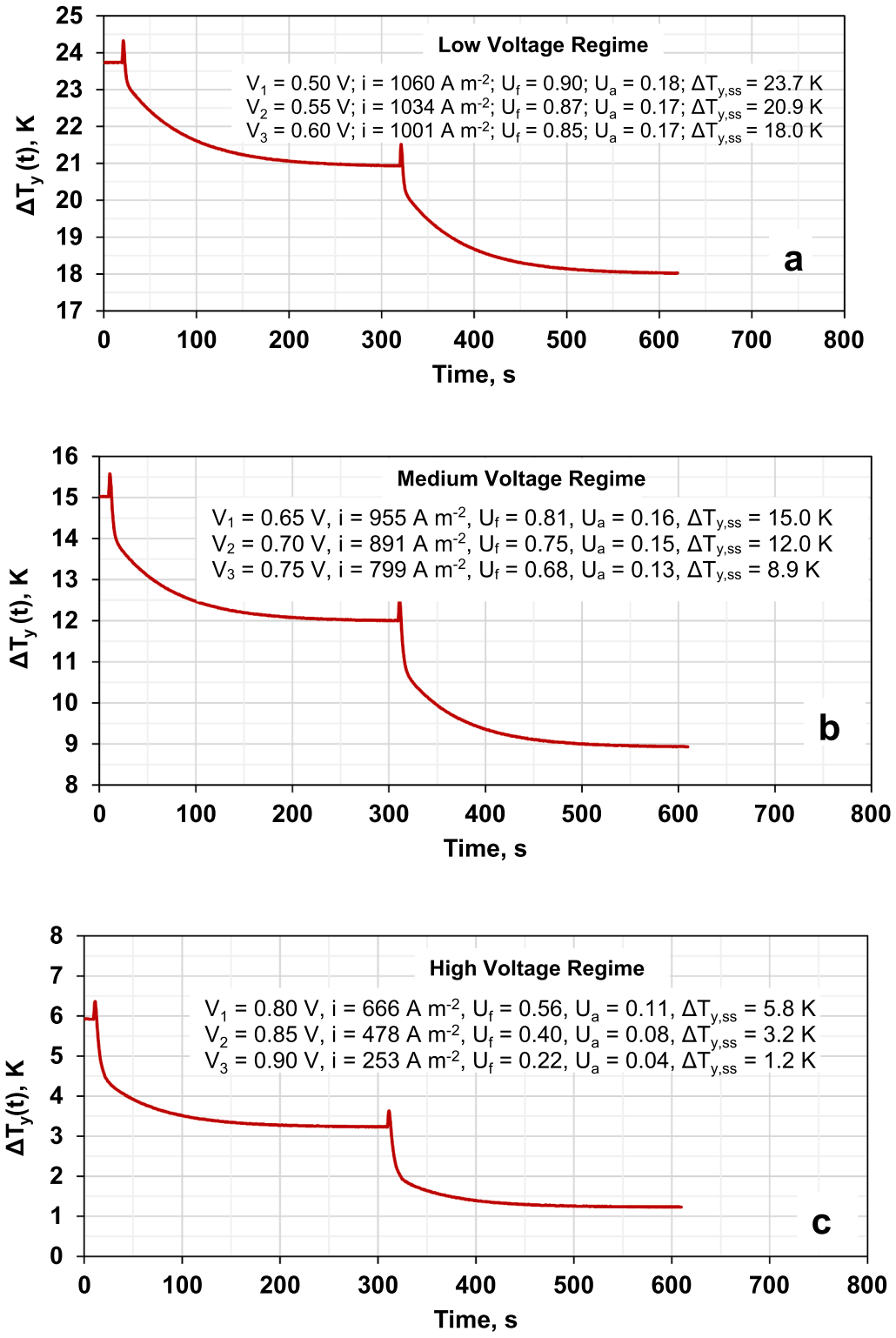

Fig. 6. The transient temperature difference (ΔT_y) response to the 0.05 V voltage interrupt for (a) low, (b) medium and (c) high operating voltage regimes.

term for SOFC thermal dynamics analysis. The in-depth insight relevant to ΔT_y as a function of time was targeted. The modelling test was based on the Voltage Interrupted Measurement method for the SOFC characterisation. The simulations were conducted for 0.05 V variation in the operating voltage at three different base voltages, including 0.50 V, 0.65 V and 0.80 V. These base voltages are representative of three operating voltage regimes including low (0.50–0.60 V), medium (0.65–0.75 V) and high (0.80–0.90 V), respectively. The voltage between the assumed regimes (e.g., 0.60–0.65 V between low and medium ranges) are considered as transition values in this study. The "voltage regime" concept is introduced in this work, for the first time to the authors' knowledge, for the SOFC performance evaluation.

The transient local temperature difference across the PEN is shown in Fig. 6 for three voltage regimes. In the three voltage regimes, the SOFC transient thermal response for the same voltage disruption was different, revealing the importance of the voltage regime's role in the analysis of

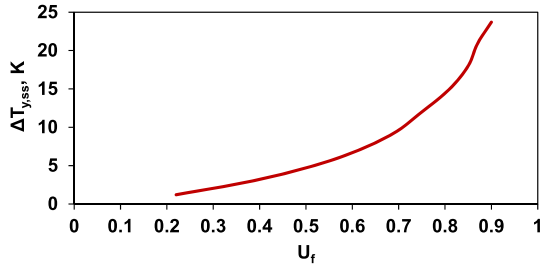

Fig. 7. The effect U_f on steady-state temperature difference across PEN.

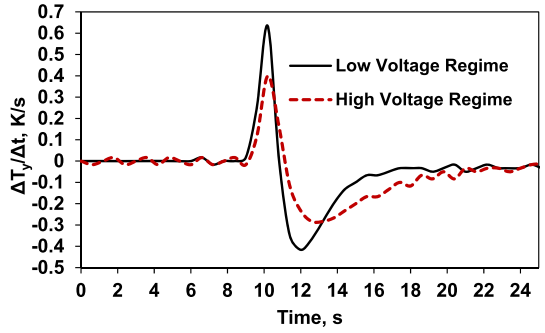

Fig. 8. Effect of operating voltage regime on the transient temperature difference (ΔT_y) response to 0.05 V voltage disturbance.

the cell thermal dynamics and control design. As can be seen in Fig. 6, in all voltage regimes the PEN experiences a lower $\Delta T_{y,ss}$ at higher operating voltages. As an example, in the low voltage regime, with a base voltage of 0.50 V, a steady temperature difference of about 24 K was achieved while it reaches 20.9 K, and 18 K for operating voltages of 0.55 V and 0.60 V, respectively. Taking voltage regimes into account, a 0.1 V variation of operating voltage may cause a max 6.3 K and 4.6 K variation in steady-state voltage at low and high voltage regimes, respectively. The $\Delta T_{y,ss}$ values were repeatable for all voltage regimes showing the model preciseness. For instance, the same $\Delta T_{y,ss}$ value was observed for V = 0.70 V regardless of whether the upper or lower regime has been used to reach 0.70 V.

Key components in the equation for achieving high electrical efficiency in SOFC-based systems include the use of high-performance materials (electrodes, electrolyte; interconnects and accompanying contact layers and coatings) and high fuel utilisation (U_f) along with minimisation of parasitic losses in the Balance-of-Plant (BoP) components. High U_f in the cell anode increases the risk of localised fuel depletion and fuel starvation due to concentration gradients, which can lead to oxidation of the most used Ni-based anode, resulting in irreparable damage to the cell and stack. The optimum operating point is a balance between the high operating voltage and high U_f, and each comes at the expense of the other due to lowering of Nernst Voltage with increasing levels of U_f with the consequence of lower operating voltage. This challenge is considered from a thermal viewpoint in this work. For each fuel utilisation target, the SOFC operation will fall in the corresponding voltage regime. The impact of the voltage regime on thermal behaviour becomes further observable when characterisation is done through the $\Delta T_{y,ss}$ versus U_f data. As shown in Fig. 7 an exponential pattern is achieved for thermal gradients against U_f revealing potentially severe thermal gradients for operation at high U_f ranges (low voltage grime). The high U_f, therefore, may damage the SOFC health through challenging thermal management in addition to the increased losses and fuel starvation concerns mentioned before.

In Fig. 8, the impact of 0.05 V variation in operating voltage on ΔT_y dynamics is shown. The undershoot and overshoot in ΔT_y profile (as a measure of temperature difference instability across the PEN) are more

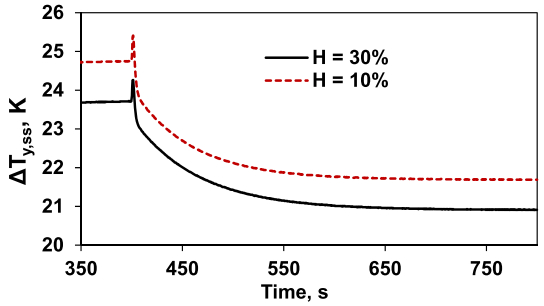

Fig. 9. Transient ΔT_y for the step changes in operating voltage (+0.05 V) for operation under two different humidity levels.

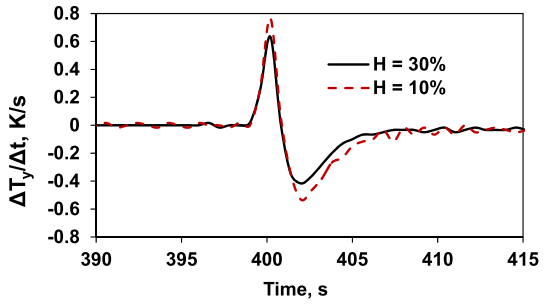

Fig. 10. Transient ΔT_y for the step changes in operating voltage (+0.05 V) for operation under two different humidity levels.

considerable at a low operating voltage regime. The settling time, however, is shorter in low voltage cases. Both overshoot/undershoot and setting time are key to thermal cycle analysis.

3.4. Voltage interruption simulation for fuel humidity impact

The steam content of fuel and anode channel is key to enhancing the longevity of the proton exchange membrane fuel cell type because of its vital role in membrane health. The SOFC fuel humidity influences its state variables, internal fuel reformation, voltage losses, and ultimately the overall performance. Moreover, steam is key to mitigate soot formation on the SOFC anode prolonging catalyst and anode active life. From the steady-state performance viewpoint, the amount of steam in the fuel channel is crucial due to its dominant role in reaction rate, OCV and voltage losses. The SOFC fuel humidity may change because of various internal and external reasons causing transient responses in the SOFC. For instance, in a system with an external reformer the steam supply may change with fuel rate, to meet the steam/carbon ratio requirement, that subsequently affect the steam content of the SOFC's feed. Similarly, the equilibrium composition of the reformer product may vary with its operating condition (i.e., temperature and pressure). Moreover, the anode exhaust gas recycling (AGR) is widely used as a practical approach for the BoP water management and fuel utilisation improvement. The recycle stream contains substantial time-dependent amount of steam in transient operations. Both AGR flowrate and its composition (two interactive operating variables) dominate the steam recycled to the anode. The former case may occur when a new AGR set point is implemented, and the latter is expected when SOFC performance fluctuates due to its operating factors, such as load disturbance, leading to the anode outlet composition variation.

The role of humidity in the SOFC thermal dynamics was investigated. A stepwise perturbation in operating voltage (±0.05 V) was applied and the results of the thermal dynamics were captured as shown in Figs. 9 and 10.

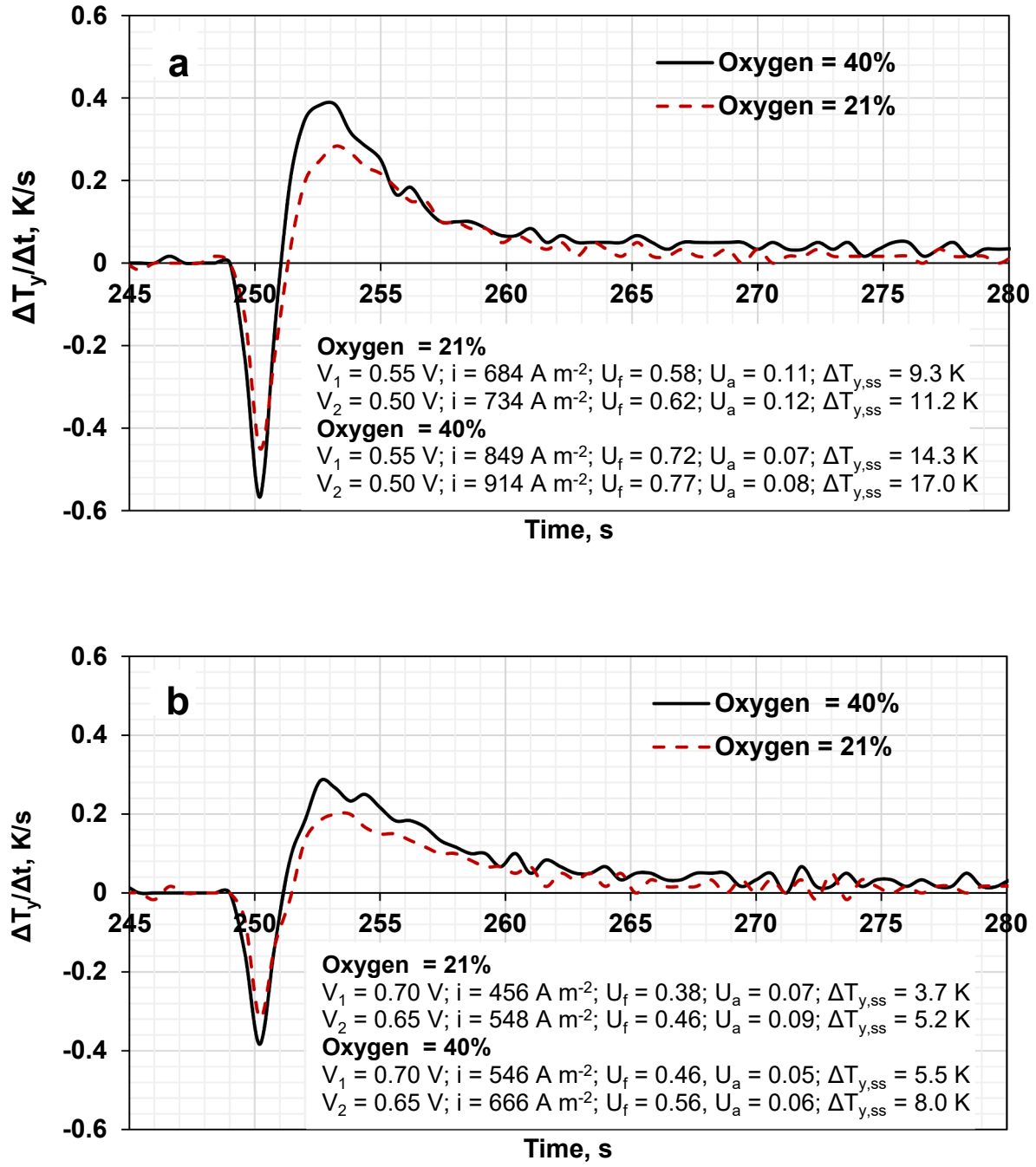

Fig. 11. Transient ΔT_y for the step (+0.05 V) changes in (a) LVR (from 0.55 V to 0.50 V) and (b) MVR (from 0.70 V to 0.65 V) operating voltage and two different oxygen levels.

3.5. Voltage interruption simulation of enriched air impact

Air is commonly used in the SOFC's cathode as the oxidant supply and coolant. The cathode side gas composition change is mainly due to the oxygen diffusion inside the PEN toward three-phase-boundary sites to feed the electrochemical reaction. The oxygen utilisation is normally low (ca. 10–20 %) in the SOFC operation. In previous works co-authors have quantitatively shown that the utilisation of oxygen-enriched air (OEA) can improve the SOFC's efficiency at cell [20] and system level [21] causing thermal behaviour concerns. The efficiency rise essentially occurs due to two reasons (i) the catalyst sites are more effectively occupied by reactants (ii) higher partial pressure of oxygen boosts the reversible OCV. Thermal improvement can be achieved as has been observed in previous studies.

The higher partial pressure of oxygen secures the availability of sufficient oxidant throughout the cathode channel minimising the oxygen starvation risk. The utilisation of upgraded air (oxygen-enriched to an optimum level) can increase the efficiency and hence (partly) compensate the parasitic losses such as power consumed for compressing (blowing) the excess air in the system. The excess air is always required for cooling purposes [25,26]. Application of OEA and even pure oxygen in the SOFC when partial oxidation reaction is the fuel reformation path is appealing as this can minimise/avoid the formation of nitrogen oxides (NO_x) pollutants. Furthermore, it decreases the concertation overpotential at cathode side. Note that the share of concertation polarisation is usually of minimum importance compared to

the other voltage losses, i.e., activation and ohmic losses. Nevertheless, oxygen and fuel starvation are serious risks for SOFC health (by accelerating degradations), and efficiency. This supports the SOFC and electrolyser integrated systems where oxygen produced by electrolysers can be deployed in the SOFC realising mentioned potentials. Even though electrolyser's main product is hydrogen, the high-quality oxygen, as its by-product, can significantly contribute to reduction of high operating cost.

The mentioned technical and economic advantages are appealing enough to motivate further investigation of the OEA deployment in the SOFC operation. The impact of oxygen quality on the SOFC thermal dynamics has not been fully understood. In this work, the SOFC transient analysis was explored, by using thermal measures, to evaluate the cells performance operated on both natural air and upgraded air.

The simulation results reveal that utilisation of the OEA in SOFC can be challenging from thermal dynamics (Fig. 11) viewpoint. The undershoot and overshoot in $\Delta T_y / \Delta t$ when OEA is used are greater than the case in which normal air is used.

4. Conclusions

In contrast to previous studies on SOFC transient behaviour [27] and particularly mode switching process investigations [28], for the first time, operating voltage regime concept was proposed and used in this work for the SOFC thermal analysis. It was shown that the voltage regime identification/consideration is significantly useful to provide detailed analysis on the SOFC thermal behaviour. The impacts of the operating strategies, including deployment of OEA and the adjustment of anode side humidity on thermal dynamics were quantitatively evaluated. It was shown that both operation variables have effect on the SOFC thermal dynamics and must be considered in multi-variable-multi-objective optimisation projects. The outcome of this study is crucial for the optimum cell design in which not only the optimum efficiency is targeted, but also a novel control strategy is aimed.

The main outcomes of this paper are:

- The thermal dynamics, in addition to steady-state temperature gradients, is of principal in evaluating thermal cycles in SOFC operation. The thermal dynamics is dominated by operating conditions. As such, it must be appraised for tens of operating scenarios requiring high-fidelity models.
- The model-based analysis shows that for the same voltage change, the SOFC thermal management will be more challenging at lower operating voltages. In contrast to the results of operating in high voltage-regime region, the low-voltage regime operation led to longer settling time, higher steady-state temperature gradient and more violent thermal dynamics.
- Running SOFC on oxygen-enriched air (up to 40 % oxygen) may result in a stronger overshoot in temperature in unstable region and higher temperature gradient across the PEN, about 50 % and 20 % higher than when natural air is utilised, for operation in low voltage and medium voltage regimes, respectively. Therefore, the benefits of oxygen-enriched air for SOFC efficiency and lifetime should be targeted at high voltage (low current) regions of V-I profiles.
- In humidity range of 10 % to 30 %, the effect of this variable on the thermal gradients and dynamics is not considerable.
- A non-linear link between Uf and thermal gradient revealed that high U_f, may damage the SOFC health by promoting the thermal management challenge, in addition to the increased voltage losses and fuel starvation concerns.

CRediT authorship contribution statement

Konstantinos Zoupalis: Investigation, Data curation, Visualization, Writing – original draft. **Amirpiran Amiri:** Conceptualization, Validation, Writing – review & editing, Supervision. **Kate Sugden:** Conceptualization, Supervision. **Michaela Kendall:** Supervision. **Kevin Kendall:** Supervision.

Declaration of Competing Interest

The authors declare that they have no known competing financial interests or personal relationships that could have appeared to influence the work reported in this paper: [Amirpiran Amiri reports financial support was provided by European Regional Development Fund. Amirpiran Amiri reports financial support was provided by Adelan Ltd.].

Data availability

The authors do not have permission to share data.

Acknowledgments

Funding for the PhD RD&I Associate for K.Z was provided from Adelan Ltd., Midlands Engine and the European Regional Development Fund as part of the "Smart Energy Network Demonstrator" based at Keele University (Grant Reference 32R16P00706).

References

[1] Kendall K, Kendall M. High-Temperature Solid Oxide Fuel Cells for the 21st Century: fundamentals. Design and Applications: Second Edition, *Academic Press* 2015. https://doi.org/10.1016/C2011-0-09278-5.
[2] Haseli Y. Maximum conversion efficiency of hydrogen fuel cells. Int J Hydrogen Energy 2018;43(18):9015–21. https://doi.org/10.1016/j.ijhydene.2018.03.076.
[3] Longo S, Cellura M, Guarino F, Brunaccini G, Ferraro M. Life cycle energy and environmental impacts of a solid oxide fuel cell micro-CHP system for residential application. Sci Total Environ 2019;685:59–73. https://doi.org/10.1016/j.scitotenv.2019.05.368.
[4] Amiri A, Tang S, Steinberger-Wilckens R, Tadé MO. Evaluation of fuel diversity in solid oxide fuel cell system. Int J Hydrogen Energy 2018;43(52):23475–87. https://doi.org/10.1016/j.ijhydene.2018.10.192.
[5] Xu Q, Ni M. Modelling of high temperature direct methanol solid oxide fuel cells. Int J Energy Res 2021;45(2):3097–112. https://doi.org/10.1002/er.6003.
[6] Selvam K, Komatsu Y, Sciazko A, Kaneko S, Shikazono N. Thermodynamic analysis of 100% system fuel utilization solid oxide fuel cell (SOFC) system fueled with ammonia. Energ Conver Manage 2021;249:114839. https://doi.org/10.1016/j.enconman.2021.114839.
[7] Brus G, Raczkowski PF, Kishimoto M, Iwai H, Szmyd JS. A microstructure-oriented mathematical model of a direct internal reforming solid oxide fuel cell. Energ Conver Manage 2020;213:112826. https://doi.org/10.1016/j.enconman.2020.112826.
[8] Yokokawa H. Current status of rapid evaluation of durability of six SOFC Stacks within Nedo Project. ECS Trans 2015;68(1):1827–36.
[9] N, Brandon, E, Ruiz-Trejo, P, Boldrin, Solid Oxide Fuel Cell Lifetime and Reliability: Critical Challenges in Fuel Cells. *Academic Press* 2017. 10.1016/B978-0-08-101102-7.00011-8.
[10] Xu Q, Guo M, Xia L, Li Z, He Q, Zhao D, et al. Temperature gradient analyses of a tubular solid oxide fuel cell fueled by methanol. Trans Tianjin University 2022. https://doi.org/10.1007/s12209-022-00331-0.
[11] Barelli L, Bidini G, Cinti G, Ottaviano A. SOFC regulation at constant temperature: experimental test and data regression study. Energ Conver Manage 2016;117:289–96. https://doi.org/10.1016/j.enconman.2016.03.028.
[12] Zeng S, Xu M, Parbey J, Yu G, Andersson M, Li Q, et al. Thermal stress analysis of a planar anode-supported solid oxide fuel cell: effects of anode porosity. Int J Hydrogen Energy 2017;42(31):20239–48. https://doi.org/10.1016/j.ijhydene.2017.05.189.
[13] Choudhary T, Sanjay R. Computational analysis of IR-SOFC: transient, thermal stress, carbon deposition and flow dependency. Int J Hydrogen Energy 2016;41(24):10212–27. https://doi.org/10.1016/j.ijhydene.2016.04.016.
[14] Razbani O, Wærnhus I, Assadi M. Experimental investigation of temperature distribution over a planar solid oxide fuel cell. Appl Energy 2013;105:155–60. https://doi.org/10.1016/j.apenergy.2012.12.062.
[15] Canavar M, Mat A, Celik S, Timurkutluk B, Kaplan Y. Investigation of temperature distribution and performance of SOFC short stack with/without machined gas channels. Int J Hydrogen Energy 2016;41(23):10030–6. https://doi.org/10.1016/j.ijhydene.2016.02.045.
[16] Sugihara S, Iwai H. Experimental investigation of temperature distribution of planar solid oxide fuel cell: effects of gas flow, power generation, and direct internal reforming. Int J Hydrogen Energy 2020;45(46):25227–39. https://doi.org/10.1016/j.ijhydene.2020.06.033.
[17] Montanini R, Quattrocchi A, Piccolo SA, Amato A, Trocino S, Zignani SC, et al. Real-time thermal imaging of solid oxide fuel cell cathode activity in working condition. Appl Opt 2016;55(25):7142.

[18] Fardadi M, McLarty DF, Jabbari F. Investigation of thermal control for different SOFC flow geometries. Appl Energy 2016;178:43–55. https://doi.org/10.1016/j.apenergy.2016.06.015.
[19] Tang S, Amiri A, Vijay P, Tadé MO. Development and validation of a computationally efficient pseudo 3D model for planar SOFC integrated with a heating furnace. Chem Eng J 2016;290:252–62. https://doi.org/10.1016/j.cej.2016.01.040.
[20] Amiri A, Tang S, Vijay P, Tadé MO. Planar solid oxide fuel cell modeling and optimization targeting the stack's temperature gradient minimization". Ind Eng Chem Res 2016;55:7446–55. https://doi.org/10.1021/acs.iecr.6b01611.
[21] Tang S, Amiri A, Tadé MO. System Level Exergy Assessment of Strategies Deployed for SOFC stack temperature regulation and thermal gradient reduction. Ind Eng Chem Res 2019;58:2258–67. https://doi.org/10.1021/acs.iecr.8b04142.
[22] Kumar P, Choudhary T, Ansari M. Thermodynamic assessment of a novel SOFC and intercooled GT integration with ORC: Energy and exergy analysis. Thermal Sci Eng Progress 2022;34:101411. https://doi.org/10.1016/j.tsep.2022.101411.
[23] Choudhary T, Sanjay R. Novel and optimal integration of SOFC-ICGT hybrid cycle: energy analysis and entropy generation minimization. Int J Hydrogen Energy 2017;42(23):15597–612. https://doi.org/10.1016/j.ijhydene.2017.04.277.
[24] Ahmed K, Föger K. Analysis of equilibrium and kinetic models of internal reforming on solid oxide fuel cell anodes: effect on voltage, current and temperature distribution. J Power Sources 2017;343:83–93. https://doi.org/10.1016/j.jpowsour.2017.01.039.
[25] Lo Faro M. Solid oxide-based electrochemical devices. Academic Press 2020. https://doi.org/10.1016/C2018-0-03867-0.
[26] N, Srisiriwat, C, Wutthithanyawat, Temperature control of an energy integrated solid oxide fuel cell system. *8th International Conference on Mechanical and Intelligent Manufacturing Technologies (ICMIMT)*, pp. 60-64 2017. DOI: 10.1109/ICMIMT.2017.7917435.
[27] Huangfu Y, Gao F, Abbas-Turki A, Bouquain D, Miraoui A. Transient dynamic and modeling parameter sensitivity analysis of 1D solid oxide fuel cell model. Energ Conver Manage 2013;71:172–85. https://doi.org/10.1016/j.enconman.2013.03.029.
[28] Li B, Wang C, Liu M, Yan J. Numerical investigation of the transient performance of a reversible solid oxide cell during the mode switching process. Energ Conver Manage 2022;268:116048. https://doi.org/10.1016/j.enconman.2022.116048.